A Fast Forward Model for Simulating EMI Scattering with Realistic Sensors and Elongated Objects

K. Sun [1], K O'Neill [1,2], I. Shamatava [1], F. Shubitidze [1] , K. D. Paulsen [1]

(1) Thayer School of Engineering, Dartmouth College,
Cummings Hall, HB 8000, Hanover NH, 03755, USA

(2) USA ERDC Cold Regions Research and Engineering Laboratory
72 Lyme Road, Hanover NH, 03755, USA

Keli.sun@dartmouth.edu

Abstract Fast solutions for UWB electromagnetic induction (EMI) scattering from fundamental object shapes are of longstanding interest for sensing of metallic objects, e.g. underground unexploded ordnance (UXO) detection and discrimination. Researchers have recently developed the general formulation for an analytical solution for EMI scattering from a spheroid. The specialization based on Small Penetration Assumption (SPA) is designed to attack the high frequency difficulties that challenge many numerical techniques. This paper uses the new analytical techniques to explore scattering from spheroids and other objects, with excitation complicated by non-uniform fields. To perform the necessary decomposition of the transmitted primary field into spheroidal modes, we represent the transmitter by a set of magnetic dipoles, which dramatically increases efficiency. The performance of the SPA solution is evaluated by comparison with results from other numerical techniques and measured data. Comparison with measured data also indicates that EMI signals from some complicated objects can be approximated by those from spheroids with similar proportions, which is promising for applications requiring fast solutions, such as inversion processing.

Keywords spheroid, EMI, scattering, SPA, GEM-3, non-uniform field, spheroidal modes

1. Introduction and review of spheroid solutions

In terms of their physical responses, some complicated but reasonably smooth, elongated objects can be approximated by a representative spheroid, when observed from some distance. The idea of approximate spheroid representation has been applied in fluid mechanics [1] and magnetic field analysis [2-4]. In the EMI frequency range (~ 10's of Hz up to ~ 100's of kHz) we are particularly attracted to the possibility, because in this band the smaller details of shape may not be important.

A great deal of work has been done in electromagnetic scattering by spheroids and analytically shaped particles, with both exact [5,6] and approximate methods [7-10]. Physical optics approximations have been used to model large particle scattering [11,12]. For scattering from more than a single particle, addition theorems were employed [13,14]. The EMI problem we are studying here is different from the previously treated problems in that (1) the frequency is very low so that the field is magneto-quasistatic (2) the scatterer is metallic, with conductivity much higher than that of the surrounding media. Tractable analytical and numerical solutions for the general EMI problem have not been available until recently [15-20]. New analytical solutions for the secondary (scattered) field from prolate spheroids were presented in [15,16], including high frequency approximations, with specialization for the SPA readily extended to oblate cases as well [17]. For our applications here, we only pursue the prolate case.

In the magneto-quasistatic EMI realm, only a scalar potential Ψ is usually required for the region surrounding a metallic scatterer. The transmitted primary (ψ^{pr}) and received secondary fields (ψ^{s}) can be expressed in that region as [16]

$$\begin{aligned} \psi^{pr} &= \frac{H_0 d}{2} \sum_{m}^{\infty} \sum_{n=m}^{\infty} \sum_{p=0}^{1} b_{pmn} P_n^m(\eta) P_n^m(\xi) T_{pm}(\phi) \\ \psi^{s} &= \frac{H_0 d}{2} \sum_{m}^{\infty} \sum_{n=m}^{\infty} \sum_{p=0}^{1} B_{pmn} P_n^m(\eta) Q_n^m(\xi) T_{pm}(\phi) \end{aligned} \quad (1)$$

where (η,ξ,ϕ) are the standard spheroidal coordinates, d is the inter-focal distance, P_n^m and Q_n^m are Associated Legendre functions, $T_{pm}(\phi)$ is $\cos(m\phi)$ for p = 0 and is $\sin(m\phi)$ for p = 1. The coefficients b_{pmn} for the primary field are known (readily calculated), and the unknown B_{pmn} must be solved for.

For high induction numbers (small skin depth) cases, one can derive relations reminiscent of impedance boundary conditions to treat the effects of internal fields. Different approaches to this are possible, the most general involving use of the magnetic field divergence equation and the normal field components and derivatives, e.g. [18,20] in the numerical realm. Alternatively, for analytical solution, all higher order terms are neglected in the governing double curl equation in [16], mostly involving tangential gradients inside the object. Then to derive an applicable gradient condition just below the scatterer's surface, the tangential field components are assumed to have functional dependencies as in a 1-D frequency domain solution with respect to the normal component, i.e. ~ $\exp\{i\alpha_n kn\}$, where k is the equivalent of wave number, here equal to $\sqrt{i\omega\sigma\mu}$ for angular frequency, electrical conductivity, and magnetic permeabilities ω, σ, and μ, respectively. In the specific case of the spheroids, α_n is unity for the azimuthal component and can be solved for analytically for the angular component H_η. With these approximations, one can solve a simple algebraic system for the unknown B_{pmn}, corresponding only to an exterior problem in the scalar potential, with no expressions involving the problematical spheroidal wave functions in the object interior. The resulting spheroid solutions for a spatially uniform primary field indicate that the SPA may produce accurate results over the entire EMI broadband, in particular where magnetic permeability μ is high, as for steel, whether skin depth is small or not. See [15,16,23] for more details.

2. Fast Decomposition of the primary field into spheroidal modes

To solve the EMI scattering problem for a spheroid using our algorithm, the key task is to decompose the known primary field Ψ^{pr} into spheroidal modes (i.e. find b_{pmn} in (1)). This is easily done for a uniform field, but otherwise may require new analytical expressions or numerical computation. In our approach, one multiplies both sides of (1) by $T_{pm}(\phi)$ $P_n^m(\eta)$ and then integrates, using established orthogonality relations for the Legendre functions to obtain

$$b_{pmn} = \frac{\int_{-1}^{1} P_n^m(\eta) \int_0^{2\pi} T_{pm}(\phi)\psi^{pr}(\eta,\xi_0,\phi)\,d\phi\,d\eta}{\frac{\alpha\pi H_0 d}{2n+1} P_n^m(\xi_0)\frac{(n+m)!}{(n-m)!}} \qquad (2)$$

where $\alpha = 1$ for $m \geq 0, p = 1$ or $m \geq 1, p = 0$, and $\alpha = 2$ for $m = 0, p = 0$. $\xi = \xi_0$ is the surface of the spheroid. At some distance away from the sensor head, the excitation field produced by most EMI transmitters can be approximated using dipole sources. For a magnetic dipole with dipole moment $\mathbf{m} = (m_x, m_y, m_z)$ at location $\mathbf{R_0} = (x_0, y_0, z_0)$, the potential and magnetic field will be [21]

$$\begin{aligned} \psi &= \frac{\mathbf{m}\cdot(\mathbf{R}-\mathbf{R_0})}{4\pi\left|\mathbf{R}-\mathbf{R_0}\right|^3} \\ \mathbf{H} &= \frac{1}{4\pi\left|\mathbf{R}-\mathbf{R_0}\right|^3}\left(\frac{3(\mathbf{R}-\mathbf{R_0})(\mathbf{R}-\mathbf{R_0})}{\left|\mathbf{R}-\mathbf{R_0}\right|^2} - \mathbf{I}\right)\cdot\mathbf{m} \end{aligned} \qquad (3)$$

At this point the potential ψ can be translated into spheroidal coordinates and be decomposed according to (2), through numerical integration.

Lab measurements were obtained using the Geophex GEM-3 broadband EMI sensor [22]. The sensor head contains two transmitting current loops with radii approximately 20cm and 10cm. The current in the inner loop is about half of that in the outer loop and it flows in the opposite direction, so that the primary field at the receiver in the head center is near zero. The primary field near the sensor is complicated and cannot be calculated analytically, so at any point of interest **H** must be calculated according to the Biot-Savart Law [21]. The potential can then be computed by integration of the magnetic field along an arbitrary path. After the values of potential on the spheroid surface are obtained, the field can be decomposed into spheroidal modes according to (2).

For a complicated ψ^{pr} such as that in the GEM-3 near field, decomposition requires numerical integration in several steps, which are too time consuming for our inversion calculations when the potential is computed as described above. Therefore we approximate the actual source by a superposition of some basic fictitious sources (i.e. point magnetic charges or dipoles), whose potential and magnetic field can be specified analytically. In keeping with the geometry of the GEM-3 sensor, the sources are distributed with azimuthal symmetry. The sensor produces fields like a magnetic dipole in the far field, and the magnetic field direction near the sensor is mainly perpendicular to its broad surfaces. Therefore we distribute the magnetic dipole sources only on the sensor surface, such that the dipoles only have a component perpendicular to the sensor head. The source distribution

contains M_1 at $\mathbf{R}_{s1} = (0,0,0)$, and M_i at $\mathbf{R}_{sij} = (\rho_i \cos(\theta_j), \rho_i \sin(\theta_j), 0)$ for $i = 2,3,\cdots N_M$, $j = 1,2,3,\cdots N_i$, where M_i are magnitudes of point dipoles and N_M and N_i are the number of rings and number of sources in each ring, respectively (Figure 1). The basic idea is to distribute the dipoles symmetrically, with different numbers at different radii. The magnetic field at position $\mathbf{R}$ will be $\mathbf{H} = \sum_{i=1}^{N_M} \frac{M_i}{4\pi} \mathbf{A_i}$ with

$$\mathbf{A_i} = \sum_{j=1}^{N_i} \frac{1}{\left|\mathbf{R} - \mathbf{R}_{sij}\right|^3} \left(\frac{3(\mathbf{R} - \mathbf{R}_{sij})(R_z - R_{sijz})}{\left|\mathbf{R} - \mathbf{R}_{sij}\right|^2} - \hat{\mathbf{z}} \right) \quad (4)$$

and $N_1 = 1$, subscripts "s" and "z" refer to source and z component.

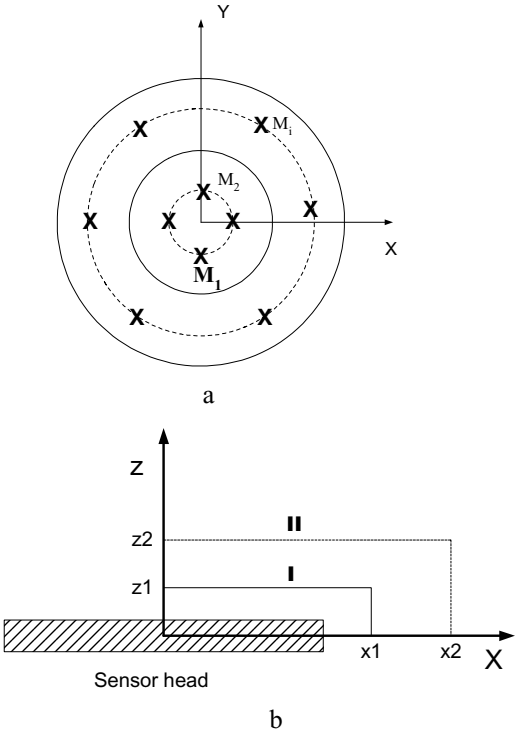

Figure 1. a) Set of dipole sources (X's); the two solid lines are the inner and outer current loop of the GEM-3 sensor. b) Control surface (I) employed to determine dipole sources and the testing surface (II) used for evaluating the accuracy of the field from these sources.

For given magnetic field at control points (on the control surface in Figure 1 b), a mean least square was employed to determine M_i, i.e. by minimizing the difference between the primary magnetic field determined by the fully detailed representation of the sensor loops and that obtained from the set of dipole sources. Then the transmitted potential of GEM-3 can be approximated by Figure 2

$$\psi^{pr} = \sum_{i=1}^{N_M} \sum_{j=1}^{N_i} \frac{M_i}{4\pi} \left(\frac{R_z - R_{sijz}}{\left|\mathbf{R} - \mathbf{R}_{sij}\right|^3} \right) \quad (5)$$

and decomposed according to (2)

3. Results and discussion

3.1 Accuracy of SPA results

The accuracy of spheroidal SPA solutions under a uniform primary field has been well studied [16,23]. As we will show below, the field from the GEM-3 sensor can be accurately represented by a set of point dipoles. So we begin here by studying the performance of SPA algorithm for objects under the non-uniform fields from dipole sources. Figure 2 shows results for a spherical object and for a 1x4 prolate spheroid, where the induction number $|k|a = \sqrt{\omega\mu\sigma}\, a$.

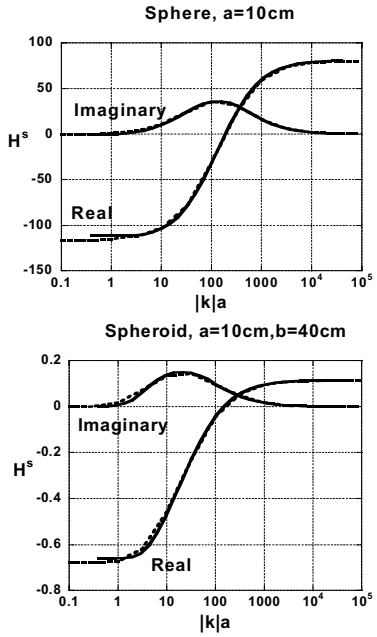

Figure 2. Scattered field from the sphere and 1x4 spheroid under dipole excitation. $\mu = 50\mu_0$. The solid lines are results obtained using the MAS and dashed lines are from the SPA.

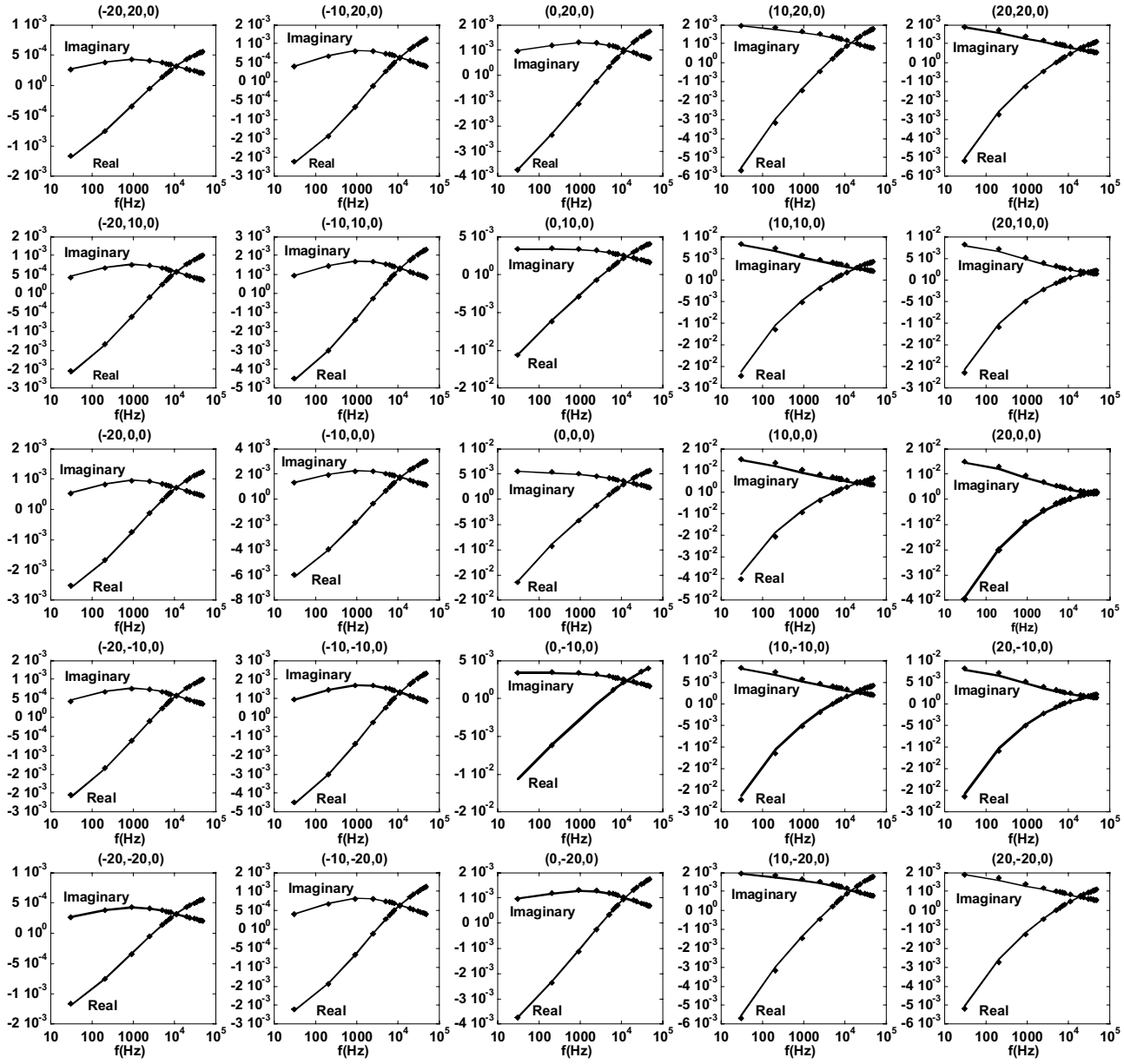

Figure 3 Comparison of SPA (markers) and MAS (lines) values (H_z^s) for a prolate spheroid (a=4cm, b=24cm) in a 5x5 grid of sensor locations. $\sigma = 4\times10^6, \mu_r = 100$, $x_0 = y_0 = 0$, $z_0 = -30cm$, $\phi_0 = 0$, $\theta_0 = \pi/4$.

Results are compared with those from a verified and complete numerical approach, namely the MAS-TSA algorithm [20] and are displayed in terms of received components in phase with the primary field (real component) and those in phase quadrature with it (imaginary component). The radius of the sphere is 10cm, the dipole is 15cm away from its center, and the scattered field was determined at the same position as the dipole transmitter. Similarly, the 1x4 prolate spheroid has the same diameter but greater length (a=10cm, b=40cm), and the dipole is at position (0,0,60cm). Although the field around the target is non-uniform, the SPA result still works very well over a wide frequency range.

To test the accuracy of SPA results for more general cases, we consider a real EMI sensor (GEM-3 developed by Geophex, Ltd.); center of the sensor is moved over a 5x5 grid on a surface above the target. The total size of the grid is 50cm by 50cm. A global coordinate system (x, y, z) on the grid has its origin at the center and z axis perpendicular

to the surface. The target center is at $(x_0, y_0, z_0) = (0, 0, z_0)$ in the global system, with units in centimeters. The orientation is described by θ_0 (the angle with z axis) and ϕ_0 (angle with x axis of the grid). At each grid point the data were calculated for 17 frequencies (distributed from 30Hz to 47,970Hz), for both real and imaginary components. An example is shown in Figure 3, with MAS results as reference [20]. Results indicate that the SPA routine is generally reliable in the frequency range studied, for non-uniform source fields, at least for these smooth and regular target shapes.

3.2 Representing the GEM-3 field with magnetic dipoles

Next we test the accuracy of the GEM-3 primary field represented by point dipoles. The "exact" magnetic field on the control and testing surfaces was calculated from direct integration around the current loops [21,22], and field values on the control surface were employed to determine point dipoles needed to represent the overall source field. Then the approximate transmitted field was compared on testing surface with that calculated from direct integration. For this example we choose the control surfaces at z = 10 cm and x = 30cm (they are in fact only lines because of the symmetry properties). The testing surfaces are at z = 15 cm and x = 45 cm. As described above, we distribute the dipole of sources in several rings. The first dipole is at the center, then the i^{th} (for $i \geq 2$) ring has radius of $\rho_i = \frac{i-1}{N_M - 1} \times 20\,cm$, where N_M is the total number of rings of sources, the number of sources in the i^{th} ring is $2i$. Figure 4 shows the comparison of approximated field with the "exact" one (namely calculated directly from current loops) on the testing surfaces. The approximated field converges to the exact one as the number of sources increases. For this case, 6 or 8 rings of dipole sources is sufficient to describe the field outside of the testing surface.

3.3 Representing complicated objects with spheroids

For EMI sensing, an arbitrary scatterer can be approximated by one or a few magnetic dipoles when viewed in the far field. However, this approximation becomes less accurate as the sensor gets closer, and in much UXO sensing we must operate in the very near field. Over most of the near field, a prolate spheroid of finite extent may be a better representative of the object than a small number of infinitesimal dipoles. To investigate the applicability of spheroidal representations for more irregular objects, we consider the response of a jagged, non-BOR piece of elongated metal scrap (Figure 5). This ordnance fragment was collected at a UXO cleanup test site. Note that the target geometry is complicated, with jagged appurtenances and different profiles in different rotations about its long axis.

Figure 6 shows the comparison between measured GEM-3 data from the piece of ordnance scrap and simulation for a best-fit prolate spheroid. The distance between the object center and the sensor is 10 cm, approximately the same as the target length. Despite the irregularities and asymmetry of the target, it produces an EMI signature similar to that of a prolate spheroid with approximately the same overall proportions. The object's lack of rotational symmetry has some effect on the signature in the orientation transverse to the primary field, but strikingly little. These results encourage further exploration of equivalent spheroid use for UXO discrimination. The scheme would rest on the assumption that one can find a sufficiently equivalent spheroid for UXO of interest and apply this equivalence in model-based inversion algorithms. For given measured EMI data, one would identify a spheroid that produces similar EMI signals by doing inversion or optimization, given that we have fast algorithm for calculating the forward EMI solution from spheroids. We expect that the scale and proportions of the spheroid will reflect the geometrical information of the measured object. One can also calculate derivatives of the forward problem solution analytically, for use in Jacobians required for inversion processing.

Pursuing this, Figure 7 shows an example real UXO, composed of a main body (magnetic), a copper band, and fins and tail with different steel. With the UXO beneath the measurement grid as shown in Figure 7, its EMI responses were measured along X and Y axis (9 points along each line) using the GEM-3 sensor and a representative spheroid was found by fitting the measured data. The EMI data from the representative spheroid are shown in Figure 8. The first 9 figures (the first and second lines) are data along X axis (y=z=0), and the second 9 figures are data along Y axis (x=z=0). Comparison with the measurement data shows that even for this complicated composite object, over an array of viewing angles by the sensor, it was still possible to find a representative spheroid which produces similar EMI response. One should note that this is a cooperative case because the steel part is much larger than other parts, and is close to the sensor, so that it dominates the response. In other orientations in which different sensor positions highlight the tail of the UXO, we expect more difficulty in matching it with a single spheroid. See [24] regarding other treatments of this same target. Overall, the very good fit observed here may not always be obtained for general composites in highly non-symmetric targets.

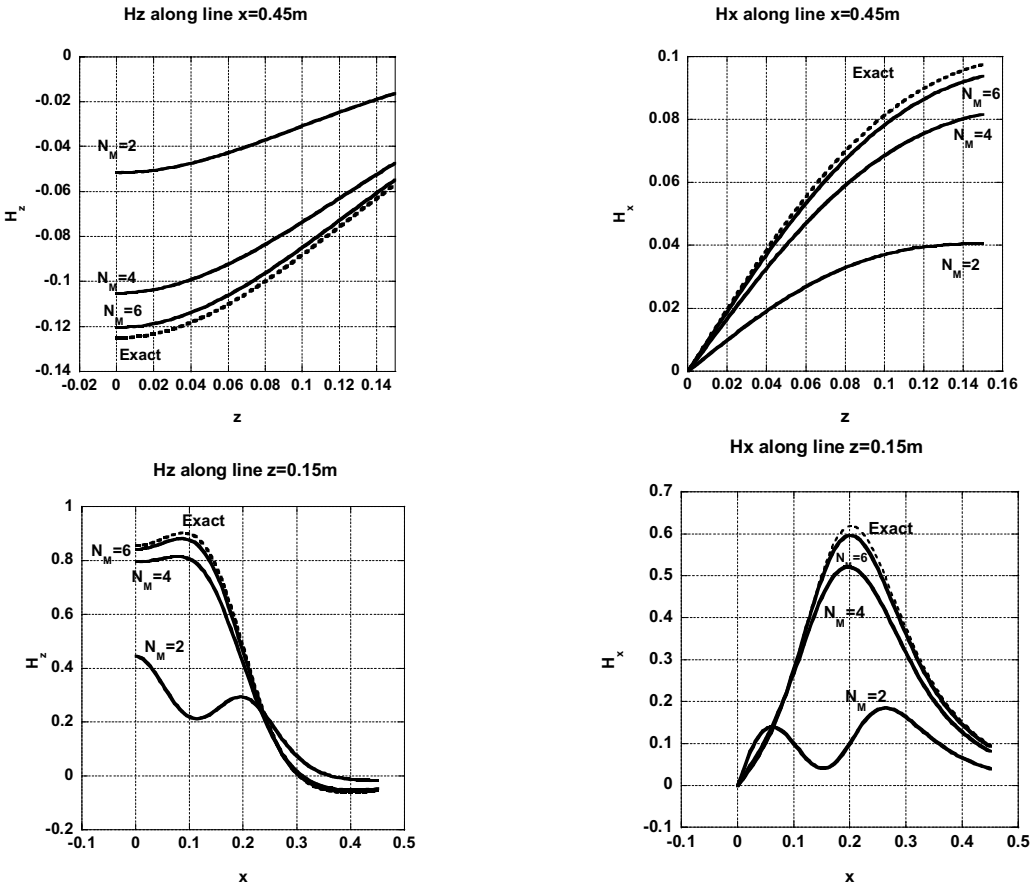

Figure 4. Convergence of the approximate field from the transmitter to the exact one, over the testing surfaces.

Figure 5. Piece of ordnance scrap on which measurements were performed, with length about 10 cm, width in one transverse direction 3~4 cm and about 2cm in the other.

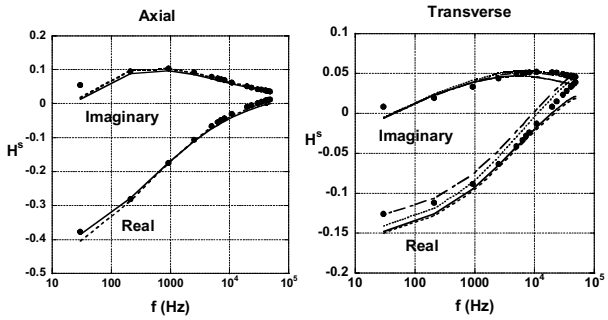

Figure 6. Comparison of the measured EMI signal from the fragment in Figure 5 (lines) with that calculated for a prolate spheroid with a = 1.25 cm, b = 5 cm, $\sigma = 2.6\times10^{6}$ (S/m), $\mu = 36\mu_0$ (dots). Different line types are for measurements from different views (i.e. up and down for the axial case, and four 90^{o} rotations about the axis for the transverse case).

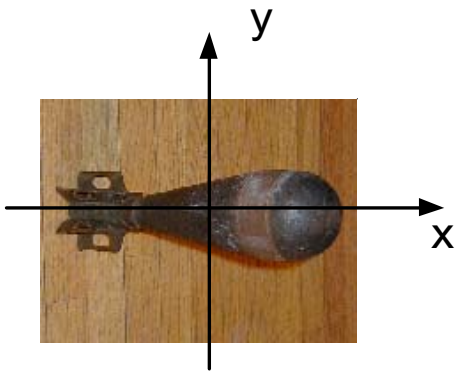

Figure 7. UXO 28 cm in length and about 8.3 cm in diameter at its widest point. Measurements are along X and Y axis, which is on a surface 22cm above the target.

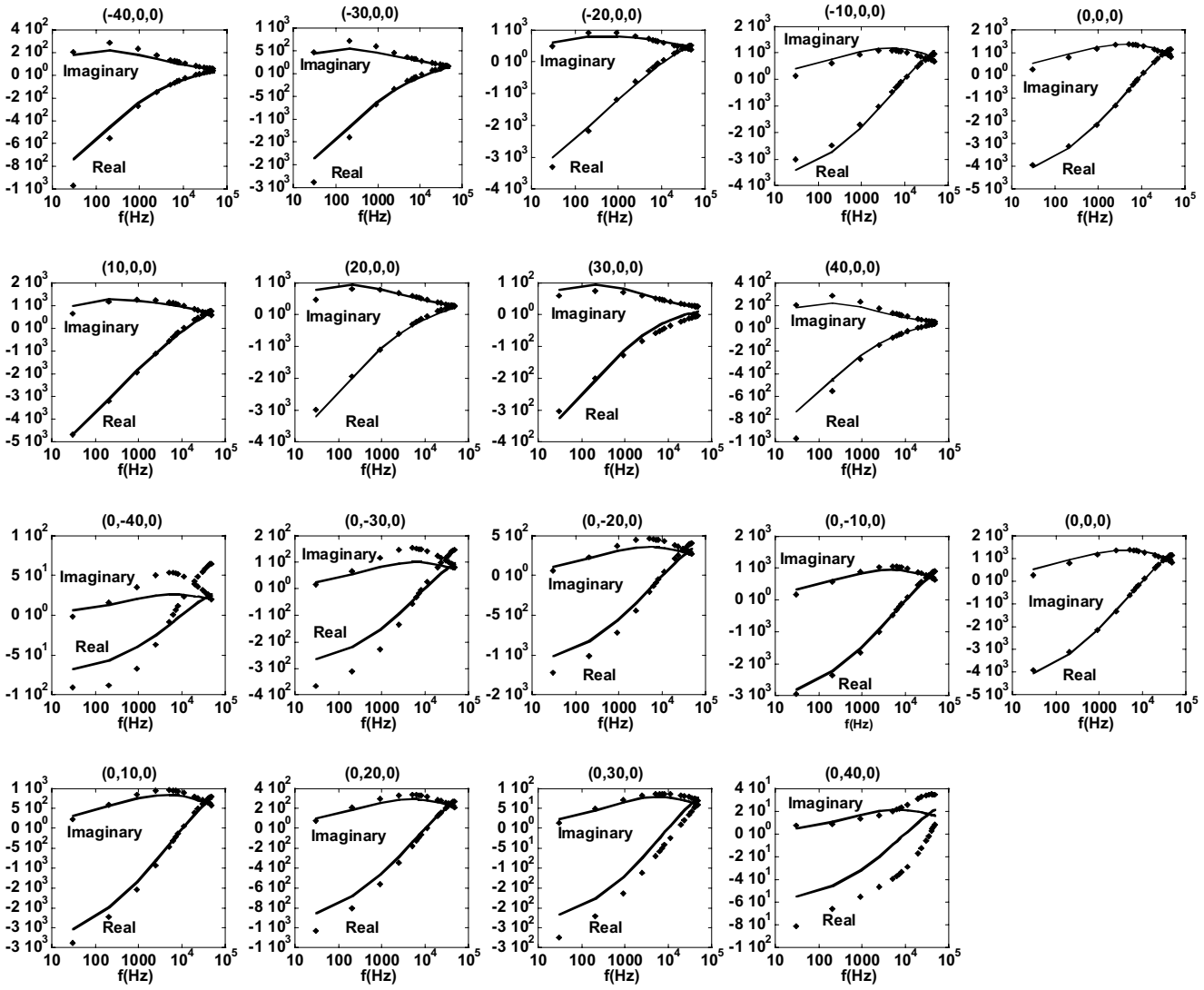

Figure 8. Scattered field H_z (in ppm) of UXO (markers) and its representative spheroid ($a = 2.2\,cm,\ b = 14cm$) along X and Y axis. $\sigma = 4\times10^6$, $\mu_r = 227$, $x_0 = 3.8cm$, $y_0 = -0.93cm$, $z_0 = -22cm$, $\phi_0 = 0$ $\theta_0 = \pi/2$.

4. Concluding Discussion

The results presented here contribute to the computational capabilities necessary for inversion of EMI measurements, in applications such as discrimination of UXO from scrap [25-27]. To approach that problem, we must be able to model both targets of interest as well as clutter. With great economy, the formulations above represent the primary field from a real sensor, using distributions of magnetic dipoles. This source construction is particularly beneficial because one can readily decompose the primary field from each contributing source into spheroidal components. For each of these, in turn, fast analytical solutions can be obtained, for steel objects. Comparison of EMI measurements and simulations suggests that even some rather irregular scatterers may be represented well by spheroidal shapes. Some limitations of the SPA type formulations can appear at low frequencies, especially for objects with low permeability [20,23]. Ultimately, this problem can be overcome by using the emerging full analytical spheroid solution, as opposed to the SPA [28, 29]. While a great many targets of interest can be idealized as bodies of revolution, future work should attack similar development of solutions for ellipsoidal shapes. With three different principal axis dimensions and correspondingly different directional scattering, they would provide the most flexible tool for inversion calculations.

Acknowledgment: This work was sponsored in part by the Strategic Environmental Research and Development Program and US Army CoE ERDC BT25 and AF25 programs. Computations were based on modifications of C. O. Ao's SPA program for uniform primary field.

References:

1. K. Sun and W. Wu, "Electrophoresis of two arbitrary axisymmetric prolate particles," Int. J. Multiphase Flow. Vol. 21, No.4, pp. 705-714, 1995.
2. S. D. Billings, J. M. Stanley and C. Youmans, "Magnetic discrimination that will satisfy regulators," UXO Forum 2002, Orlando, September 3-6, 2002.
3. K. Sun, K O'Neill, I. Shamatava, F. Shubitidze, "Application of prolate Spheroid Solutions in Simulation of EMI Scattering with Realistic Sensors and Objects, " ACES conference, Monterey, CA. pp531-537, Mar 24-28, 2003
4. K. Sun, K. O'Neill, L. liu, F. Shubitidze, I. Shamatava, K. D. Paulsen, "Analytical solutions for EMI scattering from general spheroids with application in signal inversion for UXO discrimination," Detection and Remediation Technologies for Mines and Minelike Targets VIII (or48), Part of SPIE's 17th Annual International Symposium on AeroSense, Orlando , Florida, 21–25 April 2003.
5. SH. Asano, G. Yamamoto, "Light scattering by a spheroidal particle," Appl. Opt., v.14, p. 29-49, 1975.
6. V.G. Farafonv, "Difraktsiya ploskoj e'lektromagnitnoj volny na die'lektricheskom sferoide," Diffrents. Uravn., v. 109, pp. 30-43,1983.
7. R. Pecora (Ed.), "Dynamic light scattering. Application of photo correlation spectroscopy," New York: Plenum press, 1985.
8. Van de Hulst H., "Light scattering by small particles," J. Wiley & Sons, NY,1957.
9. J.D. Klett, R.A. Sutherland, "Approximate methods for modeling the scattering properties of nonspherical particles: evaluation of the Wentzel-Kramers-Brillouin method," Appl. Opt., v.31, pp. 373-386,1992.
10. P. Latimer, "Predicated scattering by spheroids: comparison of approximate and exact methods," Photochem. Photobiol., v.19, pp.3039-3041,1980.
11. J. C. Ravey, P. Mazeron, "Light scattering in the physical optics approximation: application to large spheroids," J. Optics, v.13,pp.273-282,1982.
12. J. C. Ravey, P. Mazeron, "Light scattering by large spheroids in the physical optics approximation: numerical comparison with other approximate and exact results," J. Optics, v. 14, pp.29-41, 1983.
13. Bateshwar P. Sinha, Robet H. Macphie, "Translational additional theorems for spheroidal scaler and vector wave functions," Quart. Appl. Math., v. 38, pp. 143-158, 1980.
14. M.F.R. Cooray, I.R. Ciric, "Electromagnetic wave scattering by a system of two spheroids of arbitrary orientation," Antennas and Propagation, IEEE Transactions on, v. 37, pp. 608-618,1989.
15. H. Braunisch, C. O. Ao, K. O'Neill and J. A. Kong, "Magneto-quasistatic response of conducting and permeable prolate spheroid under axial excitation," IEEE Trans. Geosci. Remote Sensing, vol. 39, pp. 2689-2701, 2001.
16. C. O. Ao, H. Braunisch, K. O'Neill and J. A. Kong "Quasi magnetostatic solution for a conducting and permeable spheroid with arbitrary excitation", IEEE Trans, Geosci. Rem. Sens., Vol. 40, pp. 887-897, April, 2002.
17. C.O.Ao, H.Braunisch, K.O 'Neill, J.A.Kong, L.Tsang, and J.T.Johnson, "Broadband electromagnetic induction response from conducting and permeable spheroids," Proc. SPIE, vol. 4394: Detection and Remediation Technologies for Mines and Minelike Targets VI, Orlando, pp 1304-1315, April 16-20, 2001.
18. K. Sun, K. O'Neill, F. Shubitidze, S. A. Haider, and K. D. Paulsen, "Simulation of electromagnetic induction scattering from targets with negligible to moderate penetration by primary fields," IEEE Trans. Geosci. Remote Sensing, Vol. 40, pp.910-927, Apr. 2002.

19. F. Shubitidze, K. O'Neill, S. Haider, K. Sun, and K.D. Paulsen, "Application of a generalized formulation of the method of auxiliary sources to the wideband electromagnetic induction problem," IEEE Trans. Geosci. Remote Sensing, Vol. 40, pp.928-942, Apr. 2002.
20. F. Shubitidze, K O'Neill , K. Sun, I. Shamatava and K.D. Paulsen, "A combined MAS-TSA algorithm for broadband electromagnetic induction problems," ACES conference, Monterey, CA. pp566-572, Mar. 24-28,2003.
21. D. J. Jackson, "Classical electrodynamics," Wiley, New York, 3rd Edition, 1999.
22. I. J. Won, D. A. Keiswetter, D. R. Hanson, E. Novikova and T. M. Hall, "GEM-3: a monostatic broadband electromagnetic induction sensor," Jour. Envir. Eng. Geophysics, Vol. 2, No. 1, pp53-64, 1997.
23. I. Shamatava, K. O'Neill, F. Shubitidze, K. Sun and C.O. Ao, "Evaluation of approximate analytical solutions for EMI scattering from finite objects of different shapes and properties," IEEE International Geosciences and Remote Sensing Symposium and the 24th Canadian Symposium on Remote Sensing, pp1550-1552, 2002
24. F. Shubitidze, K O'Neill, I. Shamatava, K. Sun and K.D. Paulsen, "Analysis of EMI scattering to support UXO discrimination: heterogeneous and multiple objects," Detection and Remediation Technologies for Mines and Minelike Targets VIII (or48), Part of SPIE's 17th Annual International Symposium on AeroSense, , Orlando, Florida, 21–25 April 2003.
25. K. Sun, K. O'Neill, L. Liu, F. Shubitidze, I. Shamatava, "Application of Bayesian inversion of electromagnetic induction data for UXO discrimination," Symposium on the application of geophysics to environmental and engineering problems (SAGEEP03), San Antonio, TX, pp 1469-1478, April 6-10, 2003
26. K. O'Neill, K. Sun, F. Shubitidze, I. Shamatava, L. Liu, K. D. Paulsen, "Dealing with clutter in inversion and classification schemes for buried UXO discrimination," Detection and Remediation Technologies for Mines and Minelike Targets VIII (or48), Part of SPIE's 17 th Annual International Symposium on AeroSense, Orlando, Florida, 21–25 April 2003.
27. K. Sun, K. O'Neill, L. Liu, F. Shubitidze, and I. Shamatava, "Application of Bayesian inversion of scatterer shape from EMI data," IEEE International Symposium on Antennas and Propagation, Columbus, OH, June 22-27, 2003
28. B. E. Barrowes, K. O'Neill, T. M. Grzegorczyk, X. Chen and J. A. Kong, "Broadband electromagnetic induction solution for a conducting and permeable spheroid," IEEE Trans. Geosci. Remote Sensing, submitted for publication, 2003.
29. B. E. Barrowes, K. O'Neill, T. M. Grzegorczyk, J. A. Kong, "Asymptotic expansions of the prolate angular spheroidal wave function for complex size parameter," Studies in Applied Mathematics, submitted for publication, 2003

Keli Sun received his B.S., M.S. and Ph.D. degrees in Computational and Biofluid Mechanics from the Department of Mechanics and Engineering Sciences, Peking University, Beijing, P. R. China, in 1991, 1994 and 1997 respectively. As an exchange student, he also worked in the School of Pure and Applied Sciences, Tokyo University, Tokyo, Japan, from December 1995 to December 1996, studying the mobility and mechanical properties of membrane proteins in living cells. After getting his Ph.D. degree in 1997, he worked on the faculty of Tsinghua University, Beijing, P.R. China performing research and teaching biomechanics. He obtained a second Master of Science degree in Computational Electromagnetics in May 2001 from the Thayer School of Engineering at Dartmouth College in Hanover, NH. Dr. Sun is currently employed as a Research Associate in the Numerical Methods Laboratory in the Thayer School furthering his research in Computational Electromagnetics and its applications in remote sensing.

Kevin O'Neill received the B.A. magna cum laude from Cornell University, followed by M.A., M.S.E., and Ph.D. degrees from Princeton University, Department of Civil Engineering. After an NSF postdoctoral fellowship at the Thayer School of Engineering at Dartmouth College and the U.S. Army Cold Regions Research and Engineering Laboratory (CRREL), he joined CRREL as a Research Civil Engineer. His research has focused on numerical modeling of porous media transport phenomena and of geotechnically relevant electromagnetic problems. He has been a Visiting Fellow in the Department of Agronomy at Cornell University, continues since 1989 as a Visiting Scientist at the Center for Electromagnetic Theory and Applications at MIT, and since 1984 has been on the adjunct faculty of the Thayer School. Current work centers on electromagnetic remote sensing of surfaces, layers, and especially buried objects such as unexploded ordnance.

Irma Shamatava received the degree of Diploma radio physicist (M.S) from the Sukhumi branch of Tbilisi State University, Republic of Georgia, in 1994. Beginning in 1997 she joined the Staff of the Computer center, Sukhumi branch of Tbilisi State University, Republic of Georgia. During the same period she joined Department of Physics and Mathematics, as an assistant teacher. She is currently working as researcher at the Thayer School of Engineering, Dartmouth College, Hanover NH. Her research interests focus on analytical and numerical modeling of electromagnetic scattering by subsurface metallic objects.

Fridon Shubitidze received the degree of Diploma radio physicist (M.S) from the Sukhumi branch of Tbilisi State University, Republic of Georgia, in 1994 and Candidate of Sciences Ph.D degree in radio physics (applied electromagnetics) from its physics department, Tbilisi State University, Republic of Georgia, in 1997. Beginning in 1994 he was on the Research Staff of the Laboratory of Applied Electrodynamics, Tbilisi State University, Department of Physics, Republic of Georgia. At the same time he joined department of physics and mathematics, Sukhumi branch of Tbilisi State University as a senior teacher and became Associate Professor there in 1998. From 1998 to 1999 he held a postdoctoral fellowship in National Technical University of Athens, Greece, performing research in connection with computer simulation of electrostatic discharge, electrodynamics aspects of EMC, numerical modeling of conformal antennas, electromagnetic wave scattering, field visualization and identification of objects by scattered field analysis, investigation of wave propagation through anisotropy, plasma and chiral media; and innovative numerical methods. He is currently, working as Senior Research Associate at the Thayer School of Engineering, Dartmouth College, Hanover NH. His current work interests focus on numerical modeling of electromagnetic scattering by subsurface metallic objects.

Keith D. Paulsen received a B.S. from Duke University and M.S. and Ph.D. degrees from the Thayer School of Engineering, Dartmouth College, all in biomedical engineering. He was an assistant professor in electrical and computer engineering at the University of Arizona and jointly, an assistant professor in radiation oncology at the University of Arizona Health Sciences Center, and is now a professor of engineering at the Thayer School. A recipient of numerous academic and research awards and fellowships, he has carried out sponsored research for the National Science Foundation, the National Cancer Institute, the Whitaker Foundation, and the National Institute of Health. He has served on more than 10 advisory committees for the National Cancer Institute, and has chaired or organized five symposia on hyperthermic cancer treatment. He has published over 60 journal articles, over three dozen conference presentations, abstracts, and papers, and contributed chapters on electromagnetic power deposition patterns to five books. At Thayer School he is co-founder and co-manager of the Numerical Methods Laboratory. He performs research and teaches courses in computational methods for engineering and scientific problems, with particular applications in electromagnetics, subsurface object sensing, and biomedical engineering.